EFFECT OF STRENGTHENING MECHANISMS ON FATIGUE PROPERTIES OF LOW CARBON DUAL PHASE SHEET STEEL

M. KURITA, M. YAMAMOTO, K. TOYAMA, N. KOMATSUBARA and K. KUNISHIGE
Corporate Research and Development Laboratories, Sumitomo Metal Industries, LTD.
1-8 Fuso-cho, Amagasaki, Hyogo, Japan 660

ABSTRACT

This study clarifies the effect of strengthening mechanism of DP (dual phase ; ferrite plus martensite phase) steels on the fatigue properties. In order to vary the strengthening mechanism widely, addition of various alloying elements, producing high-density dislocations by low-temperature finish-rolling and pinning mobile dislocations by tempering were employed. Strain controlled and load controlled fatigue tests were performed and sub-microstructure of fatigue tested specimens was observed. Relationship among fatigue properties, mechanical properties and microstructure was discussed in comparison with ferrite plus pearlite steels.

KEYWORDS

Hot rolled sheet steel, dual phase steel, strengthening mechanism, alloying element, warm rolling, tempering, fatigue limit, endurance ratio, ferrite matrix, fatigue cracks;

INTRODUCTION

Dual phase (ferrite plus martensite microstructure) steel exhibits superior formability because it has a low yield ratio and a high elongation, and it is widely used for underbody parts such as road wheel (Takahashi et al., 1980). In most cases these parts are subjected to cyclic loading, therefore the steel needs a high fatigue strength as well as a good formability.

Fatigue properties of dual phase steels have been intensively investigated with a focus on martensite distribution by many researchers (Hayden and Floreen, 1973; Wang et al., 1987; Kawagoishi et al., 1991; Kuroki and Yamada, 1994). These studies have clarified that the endurance ratio (fatigue limit / tensile strength) of dual phase steel whose martensite is linking to each other is higher than that of dual phase steel whose martensite is isolated (Kawagoishi et al., 1991; Kuroki and Yamada, 1994).

Since some of the present authors have clarified that the fatigue limit of low carbon ferrite plus pearlite steel depends heavily on the strength of the ferrite matrix rather than the volume fraction of pearlite (Kurita et al., 1996), it is expected that the fatigue limit of low carbon dual phase steel also depends on the strength of the ferrite matrix when its microstructure is mostly ferrite. But few researchers have investigated the effect of strength of the ferrite matrix of dual phase steel on the fatigue strength.

The objective of this paper is to clarify the effect of strengthening mechanisms, mainly strengthening mechanisms of the ferrite matrix, on the fatigue properties of low carbon dual phase steel. The following strengthening methods were employed:

1)Addition of various alloying elements
2)Producing high-density dislocations by lower than Ar_3 temperature finish-rolling.
3)Pinning mobile dislocations by tempering

Load controlled and strain controlled fatigue tests were performed and sub-microstructure of fatigue tested specimens was observed. The relationship between fatigue properties and strengthening mechanism including microstructure were discussed in comparison with ferrite plus pearlite steels.

EXPERIMENTAL PROCEDURE

Materials

Various hot rolled dual phase sheet steels were prepared with various alloying elements (C, Si, P, Nb, Ti) being added to a low C-Mn-Cr-Mo base steel. Chemical compositions are given in Table 1. Fairly high alloyed base steel was selected so that the dual phase structure could be obtained even in as slow as an air cooling condition (Kunishige et al., 1979). They were all laboratory melted. Ingots were forged to slabs approximately 30 mm in thickness. After heated to 1473K, the slabs were finish-rolled at 1153K into 6mm thick sheets.

The coupon slabs of the base steel and Si-added steel were used and they were finish-rolled at low temperatures, 1033K and 1073K (codes AL and CL) to produce high-density dislocations in the ferrite matrix.

In addition, the sheet steels of the base steel and Si-added steel were tempered at 473K (codes AX and CX) and 573K (codes AY and CY) for 30minutes to pin the mobile dislocations generated when martensite transformation occurred.

Table 1 Chemical compositions (mass%)

Code	C	Si	Mn	P	S	Cr	Mo	Others
A(the base), AL, AX, AY	0.05	0.51	1.55	0.021	0.001	0.70	0.26	
B(carbon)	0.10	0.50	1.51	0.020	0.001	0.69	0.25	
C(silicon), CL, CX, CY	0.05	1.50	1.52	0.019	0.001	0.71	0.26	
D(phosphorus)	0.05	0.51	1.54	0.077	0.001	0.72	0.26	
E(niobium)	0.05	0.49	1.46	0.019	0.002	0.70	0.25	Nb:0.024
F(titanium)	0.05	0.51	1.47	0.018	0.001	0.69	0.25	Ti:0.050

Test Specimen

The test specimen is illustrated in Fig. 1. The axial loading direction of the specimen was chosen parallel to the rolling direction of steel sheets. The surface of the specimen was mechanically polished by using 700 grit emery paper in the axial direction to remove any circumferential scratches and machine marks. Some of the test pieces were buffed for the observation of fatigue cracks and slip bands.

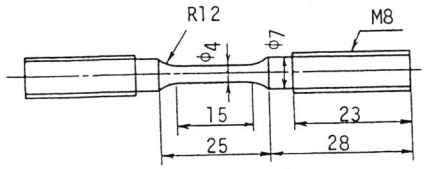

Fig. 1 Shape and size of fatigue test specimen

Fatigue Tests

Load controlled fatigue test : Load controlled fatigue test was carried out to obtain the fatigue limit. The testing machine has an electro hydraulic servo controlled system. Fatigue test was performed under load controlled condition at a stress ratio of -1 and frequencies of 15 to 20 Hz.

Strain controlled fatigue test : Strain controlled fatigue test was carried out to obtain cyclic stress response curve, which indicates the resistance of the steel to cyclic deformation. The same testing machine described in the previous section was employed and fatigue test was performed under strain controlled condition at a strain ratio of 0 and frequencies of 2 to 4 Hz. The strain ratio was chosen so as to ensure that it would not buckle under compressive strain. The strain was monitored with a 12.5 mm extensometer which was attached to the gauge section of the test specimen.

RESULTS

Microstructure and Mechanical Properties

Microstructures are shown in Fig. 2. Microstructural characteristics are listed in Table 2. All the grain size of ferrite were almost the same irrespective of additional element, while the volume fractions of second hard phase, Vf(H), were not the same. Vf(H) of carbon added steel was two times as large as that of other steels. The hardness of ferrite and martensite did not change largely with tempering temperature.

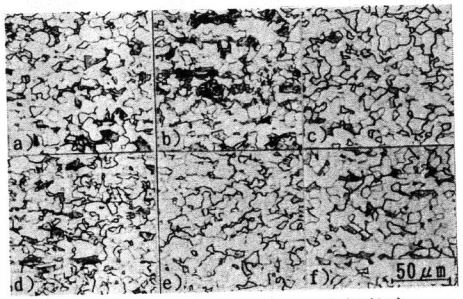

(a)A(base) (b)B(C) (c)C(Si)
(d)F(Ti) (e)CL(Si:L-T.F-R.) (f)CY(Si:573K Temp.)

Fig. 2 Microstructure of steels tested

Mechanical properties are listed in Table 3. All of the alloying elements increased both the yield stress and the tensile strength. Low-temperature finish-rolling increased the yield stress of the base and Si-added steels by 42MPa and 67MPa, respectively. However, the tensile strength increased by a small amount; 20MPa and 21MPa. Tempering changed mechanical properties nearly in the same way as low-temperature finish-rolling: Yield stress markedly increased with tempering temperature, while tensile strength increased slightly.

Table 2 Microstructual characteristics

Code	d (μm)	Vf(H) (%)	HV(H) (HV0.1)	HV(F) (HV0.02)	note
A	5.6	17	384	155	As rolled
B	6.5	34	406	185	
C	6.3	13	448	193	
D	6.1	16	427	179	
E	5.8	14	370	196	
F	6.3	9	460	202	
AL	6.3	17	336	181	Low-temperature finish-rolled
CL	6.3	14	540	215	
AX	6.0	16	389	154	Tempered at 473K
CX	6.3	13	482	191	
AY	5.8	17	381	151	Tempered at 573K
CY	6.4	14	468	188	

d:Average grain diameter
Vf(H):Volume fraction of 2nd hard phase
HV(H):Vickers hardness of 2nd hard phase
HV(F):Vickers hardness of ferrite

Table 3 Mechanical properties

Code	σ_y (MPa)	σ_B (MPa)	ε_f (%)
A	297	581	28.3
B	379	736	22.2
C	338	647	27.3
D	302	603	27.8
E	410	652	26.9
F	427	649	25.0
AL	339	601	22.8
CL	405	668	22.6
AX	351	600	29.0
CX	404	661	29.0
AY	414	588	29.3
CY	476	653	28.3

σ_y:Yield stress
σ_B:Tensile strength
ε_f:Elongation

The examples of TEM micrographs are shown in Fig. 3. High-density dislocations can be observed in the ferrite matrix in all steels. Figure 3(b) shows the fine TiC precipitates in the ferrite matrix of Ti-added steel. Figure 3(c) shows high-density tangled dislocations in low-temperature finish-rolled Si-added steel. This dislocation structure explains the high yield stress of tempered steels.

No carbide precipitates were observed in the ferrite matrix of all the as-rolled and tempered steels except Ti-added and Nb-added steels.

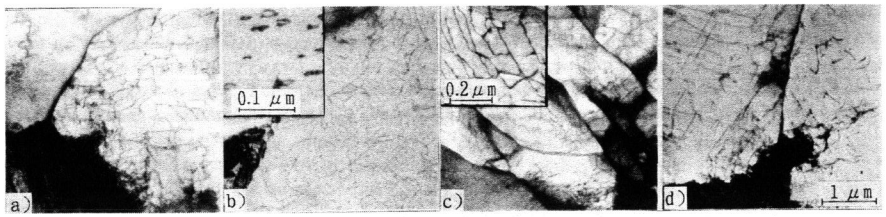

(a)A(base) (b)F(Ti) (c)CL(Si:L-T.F-R.) (d)CY(Si:573K Temp.)

Fig. 3 TEM micrographs of the steels before fatigue test

Load Controlled Fatigue Test

Figure 4 shows relationship between stress amplitude and the number of cycles to failure. Fatigue limit obtained from Fig. 4, and the endurance ratio (the ratio of fatigue limit / tensile strength) are listed in Table 4. In addition, the relationship between tensile strength and fatigue limit for as-rolled steels is shown in Fig. 5. The endurance ratio varied widely from 0.41 to 0.61 depending on the type of steel. The carbon added steel exhibited a low endurance ratio; the addition of carbon increased tensile strength without increasing fatigue limit. On the other hand, the silicon, phosphorus, niobium and titanium added steels exhibited high endurance ratios. These results indicate that solid solution or precipitation elements increase fatigue limit considerably with a small increase in tensile strength.

Low-temperature finish-rolling and tempering at 473K and 573K changed the fatigue limit slightly.

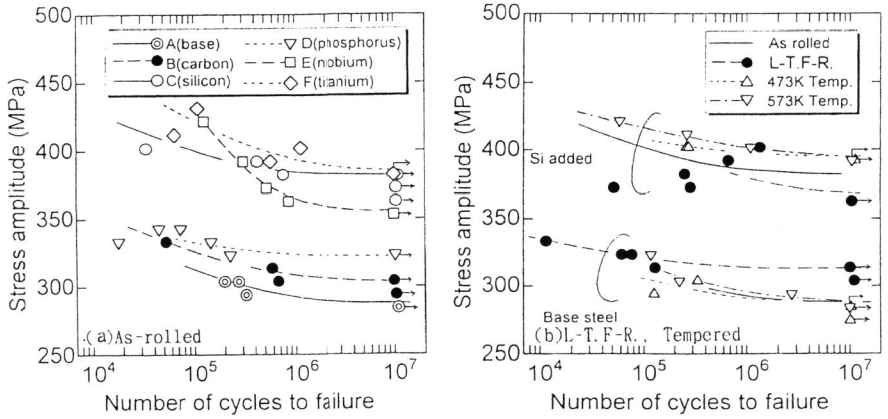

Fig. 4 Relationship between stress amplitude and number of cycles to failure

Table 4 Fatigue limit

Code	Fatigue limit σ_w (MPa)	σ_w / σ_B
A	289	0.50
B	304	0.41
C	378	0.58
D	323	0.54
E	358	0.55
F	387	0.60
AL	319	0.53
CL	368	0.55
AX	289	0.48
CX	397	0.60
AY	289	0.49
CY	397	0.61

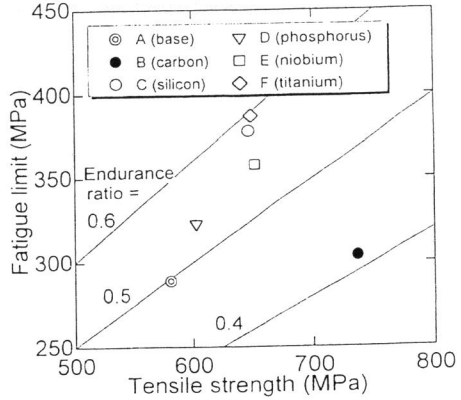

Fig. 5 Relationship between tensile strength and fatigue limit for as-rolled steels

Strain Controlled Fatigue Test

Figure 6 shows the change of stress amplitude with the number of cycles under strain control. The stress amplitude at the beginning of fatigue life had a tendency to increase proportionally with the yield stress. As shown in Fig.6(a), all of the as-rolled steels and low-temperature finish-rolled steels exhibited cyclic hardening For tempered steels, however, the cyclic behavior depended on the tempering temperature. As tempering temperature became high, the tempered steels exhibited cyclic softening to larger extent. In addition, the most noted fact is that all the stress amplitudes toward the half fatigue life were almost the same independent of tempering temperature as shown in Fig.6(b).

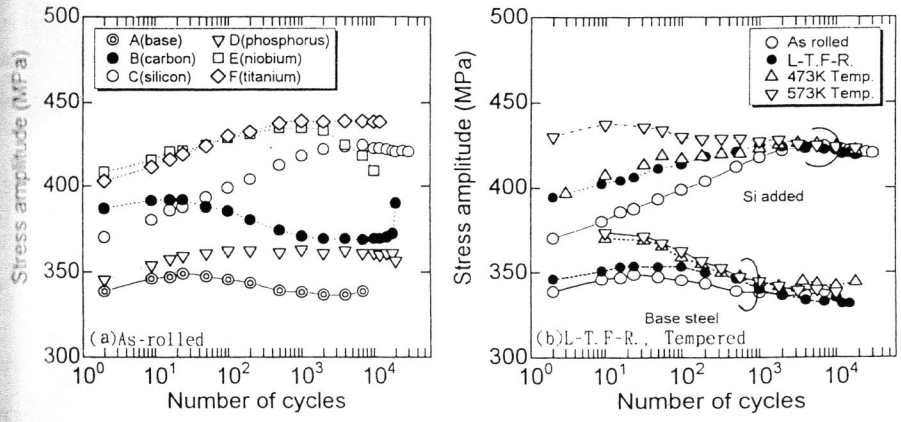

Fig. 6 Change in stress amplitude with number of cycles ($\Delta \varepsilon_t$=0.6%)

TEM Micrographs of Submicrostructure after Fatigue Test

Figures 7(a),(b),(c) and (d) show TEM micrographs of as-rolled steels after fatigue test. Dislocation cells or dislocation walls are observed clearly in all of the steels except Ti- or Nb-added steel. In addition, TiC precipitates are seen in Fig.7(d). This indicates that these precipitates were stable and not dissolved during the cyclic deformation. The behavior and role of TiC precipitates in dual phase steel are almost the same as those in the ferrite plus pearlite steels (Toyama and Kurita, 1991).

Figure 7(e) shows TEM micrographs of low-temperature finish-rolled steel. Figures 7(f) and (g) show those of tempered steels. Dislocation cells or dislocation walls are observed in all of the three steels.

In addition, submicrostructure of specimen which was fatigued in load controlled fatigue test was compared with that in strain controlled fatigue test. The main differences between these fatigued specimens are the magnitude of loaded stress amplitude and the resultant number of cycles to failure. Figure 7(h) shows submicrostructure of the 573K tempered steel after 2.65×10^5 cycles at 412 MPa. This micrograph shows that this dislocation structure was almost similar to that in Fig.7(g). This indicates that the morphology of dislocation structure formed by cyclic deformation hardly depends on the stress amplitude or the number of cycles.

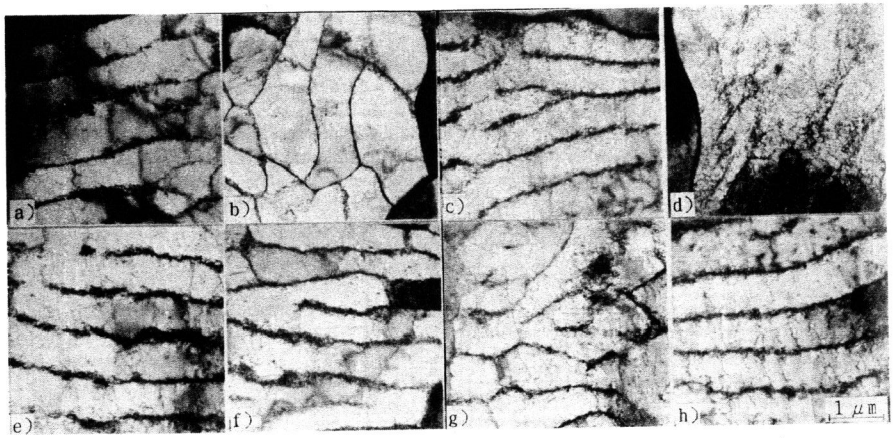

(a)A(Nf=8.5×10^3) (b)B(Nf=2.1×10^4) (c)C(Nf=3.4×10^4) (d)F(Nf=1.4×10^4)
(e)CL(Nf=1.9×10^4) (f)CX(Nf=2.3×10^4) (g)CY(Nf=2.4×10^4) (h)CY(412MPa, Nf=2.7×10^5)

Fig. 7 TEM micrographs of the steels after fatigue test($\Delta\varepsilon_t$=0.6%, except (8))

DISCUSSION

The Effect of Alloying Elements on Fatigue Strength

From the viewpoint of materials design, it is of vital importance to establish the quantitative relationship between mechanical properties and fatigue limit. In the previous study, the relationship between tensile strength and fatigue limit was summarized and formulated by using the increases in tensile strength and in fatigue limit from the base steel (Kurita et al., 1996). In this study, the results of fatigue test were summarized in the same way as shown in Fig. 8. Here, the results of tempered steels were excluded because the increase in tensile strength by tempering was very small. Figure 8 shows that the ratio of $\Delta\sigma_w/\Delta\sigma_B$ is small for the addition of carbon, while as large as 1.0 to 1.5 for the addition of Si, P, Nb and Ti. These results indicate that

strengthening of the ferrite matrix by solid solution or precipitation element is effective in increasing the endurance ratio, while increasing of the martensite volume fraction is not effective. These results can be explained by the observation of surface of fatigued specimens. Figure 9 shows that the fatigue cracks initiated at the ferrite matrix in the vicinity of martensite. Moreover, Figure 9(a) shows that the fatigue cracks propagated avoiding martensite. It is concluded that the fatigue limit heavily depends on the resistance of ferrite against initiation and propagation of fatigue cracks.

In addition, these results indicate that solid solution and precipitation elements can increase the resistance to both tensile deformation and cyclic deformation by the same amount. Besides, the ratio of $\Delta\sigma_w/\Delta\sigma_B$ of low carbon ferrite plus pearlite steel was founded to be 0.91 for solid solution strengthening and 0.97 for precipitation strengthening (Kurita et al., 1996). These results indicate that the ratio, $\Delta\sigma_w/\Delta\sigma_B$, is almost constant, being independent of not only the kind of additional element but also the kind of the second hard phase, martensite or pearlite. This is presumably because both in the present study and in the previous study the carbon content is low, resulting in the volume fraction of the second hard phase being too small to affect the behavior of fatigue cracks.

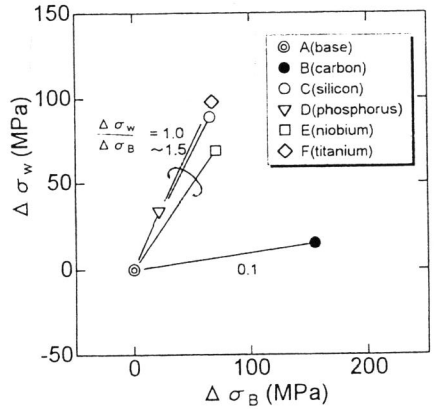

Fig. 8 Relationship between increase in tensile strength and that in fatigue limit for as-rolled steels

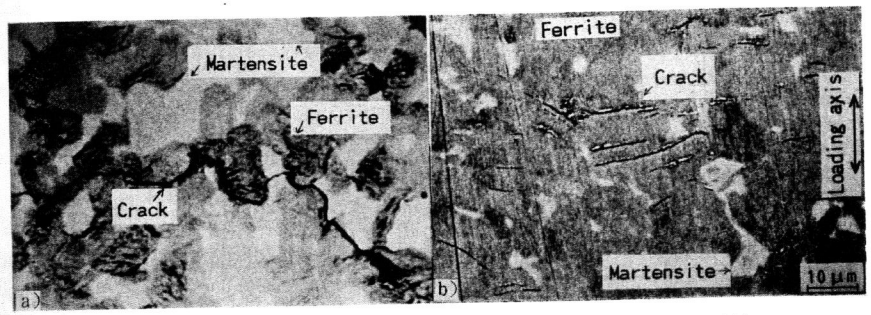

(a)B(C, σa=333MPa, Nf=8.2×10^4) (b)E(Nb, $\Delta\varepsilon_t$=0.6%, Nf=1.1×10^4)

Fig. 9 SEM micrographs of surfaces of test steels after fatigue test

The Effect of Tempering on the Fatigue Strength

As shown in Table 3, the yield stress was increased by tempering at 473K and 573K. This is because dislocations generated when martensite transformation occurred were pinned by solute atoms such as C and N. However, the tempering increased the fatigue limit to a very small extent for the base and Si-added steels.

As shown in Fig.6, tempered steels exhibited higher stress amplitude at the beginning of cyclic deformation than as-rolled steels. The difference between stress amplitude of these steels, however, decreased with the number of cycles, and became very small toward the half fatigue life. This indicates that the resistance of ferrite against cyclic movement of dislocations at the final stage of fatigue life did not differ with tempering temperature. The mechanism can be explained in terms of the submicrostructural changes shown in Fig.3(d) and Fig.7(g). These figures show that dislocation structures of tempered steels were rearranged during cyclic deformation, presumably reducing the resistance against cyclic movement of dislocations. Considering the fact that the as-rolled steels exhibited cyclic hardening due to dislocation tangling, the way in which dislocation cells or walls form in the tempered steels is considered as follows; dislocations are released from the pinning effect by solute atoms, and then the dislocations become tangled. Though above-mentioned explanation was deduced from the results of strain controlled fatigue testing, this explanation is applicable to the results of the load controlled fatigue test since dislocation structure formed by cyclic deformation in the load controlled fatigue test was nearly the same as that in the strain controlled fatigue test. It is concluded that the small increase in fatigue limit by tempering was attributed to the low resistance of ferrite against rearrangement of dislocation. Solute atoms were less effective in pinning dislocations under cyclic deformation than precipitates such as TiC and NbC.

CONCLUSIONS

In order to clarify the effect of strengthening mechanisms on fatigue properties, fatigue tests and TEM observation were carried out on steels strengthened by various methods. The following results were obtained:
(1)Addition of solid solution or precipitation strengthening elements increased the fatigue limit, effectively leading to a high endurance ratio. On the other hand, the addition of carbon, increasing the volume fraction of martensite, did not increase the fatigue limit. This is because only the former elements strengthen the ferrite matrix where fatigue cracks initiate.
(2)Production of high-density dislocations in the ferrite matrix by low-temperature finish-rolling and pinning of the mobile dislocations by tempering both increased yield stress significantly, but these strengthening mechanisms increased the fatigue limit by a small amount. This is because the dislocation structures formed by these strengthening mechanisms are easily rearranged during cyclic deformation.
(3)Thus it is concluded that the strengthening of the ferrite matrix by solid solution or the precipitation hardening is essential to increase the fatigue limit and endurance ratio of low carbon dual phase steel as well as low carbon ferrite plus pearlite steel.

REFERENCES

Hayden, H. W. and Floreen, S. (1973). Met. Trans., 41, 561
Kawagoishi, N., Nishitani and H., Toyohiro, (1991). Trans. JSME, Ser. A, 57, 2866
Kunishige, K., Takahashi, M., Sugisawa, S. and Masui, Y. (1979). Tetsu-to-Hagane, 76, 414
Kurita, M., Yamamoto, M., Toyama, K., Nomura, S. and Kunishige, K (1996). ISIJ Int., 36, 481
Kuroki, T. and Yamada, T. (1994). Trans. JSME, Ser. A, 60, 1498
Takahashi, M., Kunishige, K. and Okamoto A. (1980). Bulletin of JIM, 19, 10
Toyama, K. and Kurita, M. (1991), ASME MD-Vol.28, 185
Wang, Z., Wang, G., Ke, W. and He, H. (1987). Mat. Sci. and Eng., 91, 39